Predicting the strength of 3D-printed conductive composite under tensile load: A probabilistic modeling and experimental study

Nassima Naboulsi, Fatima Majid, Taoufik Hachimi, Soufyan Dadoun
Laboratory of Nuclear, Atomic, Molecular, Mechanical and Energetic Physics, Chouaib Doukkali University, El jadida, Morocco
naboulsi.n@ucd.ac.ma; majid.f@ucd.ac.ma; hachtaoufik@gmail.com; dadounsoufyan@gmail.com

Najoua Barhoumi, Kaouther Khlifi
Laboratory of mechanics materials and processes, National high school of engineering of Tunis (ENSIT), 5 rue Taha HussienMonfleury, 1089 Tunis Bab Alleoua, Tunis
najoua.barhoumi@ipeiem.utm.tn; khlifi.kaouthar@yahoo.fr

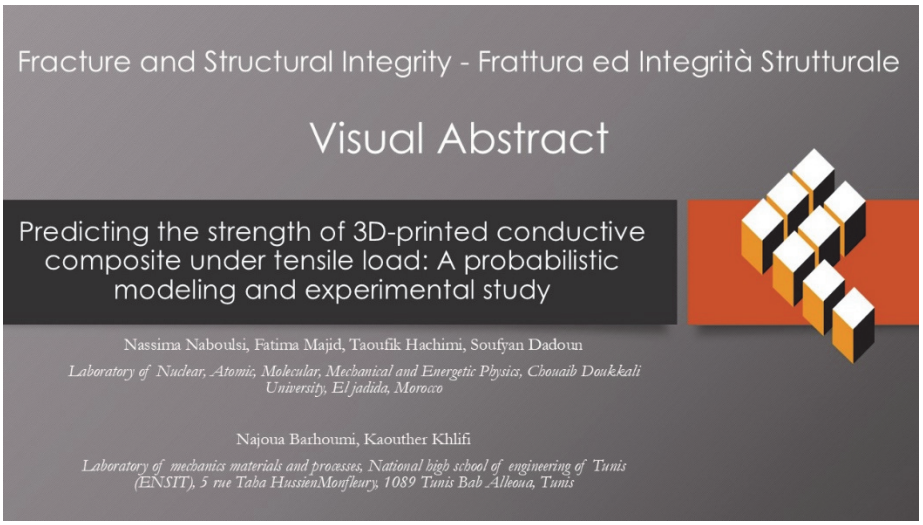

Citation: Naboulsi, N., Majid, F., Hachimi, T., Dadoun, S., Barhoumi, N, Khlifi, K, Predicting the strength of 3D-Printed Conductive Composite Under Tensile Load: A Probabilistic Modeling and Experimental Study, Fracture and Structural Integrity, 72 (2025) 247-262.

Received: 09.02.2025
Accepted: 22.03.2025
Published: 24.03.2025
Issue: 04.2025

KEYWORDS. Composite Material, PLA-CB, Durability, Mechanical behavior, Reliability, Weibull.

INTRODUCTION

In recent years, conductor polymers have attracted more interest due to their ability to opened to various fields, including electronics [1], energy [2] , and multifunctional materials [3]. Thanks to their particular combination of electrical characteristics, flexibility, and light weight, they prove an ideal choice for a diverse range of applications, including sensors, electronic devices and integrated circuits [4], especially by using 3D printing technology , it has recently become possible to adjust electrical and mechanical characteristics into personalized structures [5],while also taking advantage of the financial and environmental benefits offered by additive printing [6].

Conductive polymers are usually classified into two main categories. The first category includes intrinsically conductive polymers (ICPs), such as polyaniline and polypyrrole, which have intrinsic electrical conductivity due to their specific chemical structure. These polymers have molecular chains with conjugated electron systems that allow the movement of electrical charges without the need to add external materials [7]. The second category is called conductive polymer composites (PCCs), which are made by combining conductive fillers, such as carbon black or carbon nanotubes, in an insulating polymer matrix [8].

The polymer composite conductors attract particular interest within these two categories due to their flexibility in selecting base materials and conductor charges which allows researchers to adjust their features to specific applications. In this regard, our research focuses on PLA-CB, which employs 3D printing technology by filament deposition (FFF) to create an ideal balance between environmental preservation and electrical functionality. The objective is to determine the mechanical properties of PLA-CB and assess its behavior under many different conditions in order to better understand its potential for both functional and multifunctional applications.

This paper investigates the impact of crosshead speed and strain rate, along with the effect of various notch geometries (single or double, U-shaped or V-shaped and central hole) on the mechanical properties and reliability of the PLA-CB. A hybrid approach was implemented using deterministic analysis to study mechanical characteristics, and probabilistic analysis based on Weibull distribution to study the probability of failure and survival under different conditions. In addition, we analyzed structural orientation of the printing layers (0° and 45°) using SEM, with the goal of improving our understanding of fracture mechanisms and their relationship to the material's microstructure. Through this study of microstructure, the authors can examine how the orientation of layers affects stress distribution and areas of weakness, offering recommendations for improving the mechanical properties of printed components.

Several previous studies have investigated the mechanical and electrical behavior of conductive polymers [9]. For example, [10] demonstrated that the addition of annealing improves the properties of 3D printed graphene-reinforced PLA composite by increasing crystallinity, electrical conductivity and mechanical strength. In other studies, such as [11], the thermal and electrical properties of PLA/PP hybrid biocomposites containing active carbon were determined, and the effects of adding active carbon was investigated. Finally, [12] employed a new technique to improve both the mechanical and electrical conductivity PLA-CB composites. By applying a tensile strain along with a thermal treatment, the researchers observed a significant increase in electrical conductivity.

The originality of this work lies in its comprehensive and integrated approach to studying the mechanical behavior of PLA-CB. It combines deterministic mechanical, probabilistic analysis using Weibull model, and microstructural analysis. This new approach opens up new possibilities for designing highly functional, multifunctional components, even for demanding applications such as electronic printing, smart sensors, and lightweight structures.

EXPERIMENTAL SECTION

Studied Material

The conductive PLA-CB filament used in this study is refers to a composite material combining conventional PLA with 40% conductive black carbon fillers [13], [14]. The filament used is of the highest quality, processed through a reliable extrusion system with precise control of the melting temperature to ensure optimal testing conditions [15], [16]. It is frequently used to create printed objects with electrical properties. Its melting temperature is (200-230°C), making it suitable for low-current applications. This filament can be used to create objects with electrical properties, such as printed circuit boards or sensors. However, its mechanical strength is often lower than that of standard PLA due to the addition of conductive particles. These filaments are ideal for prototypes or projects requiring small-scale electrical conductivity. Its resistance is 1,8 KΩ for 10cm of filament with diameter of 1,75mm [17].

Physical-chemical characterization - X-Ray diffraction (XRD)

X-ray diffraction patterns were obtained under ambient laboratory conditions and normal atmospheric pressure. The analysis was performed using a Bruker-AXS diffractometer, model D8, calibrated with the following parameters in Tab. 1. The crystallite size was measured using specialized High Score Plus software, for precise analysis of diffraction data. In addition, Origin software was used to plot and model the molecules studied, providing detailed visualizations and clear interpretation of molecular structures of the samples analyzed. Fig. 1 shows the BRUKER-AXS D8 X-ray diffraction machine alongside the printed sample size prepared for XRD analysis.

Diffraction interval	Angular step	Scanning time per step	Radiation source	wavelengths	Generator Voltage	Generator Current	Goniometer radius
5° ≤ 2θ ≤ 70°	0.061°	192 seconds	Copper anode	Kα1 = 1.5406 Å Kα2 = 1.54443 Å	50 kV	20 mA	240 mm

Table 1: Diffraction parameters for the Bruker-AXS diffractometer.

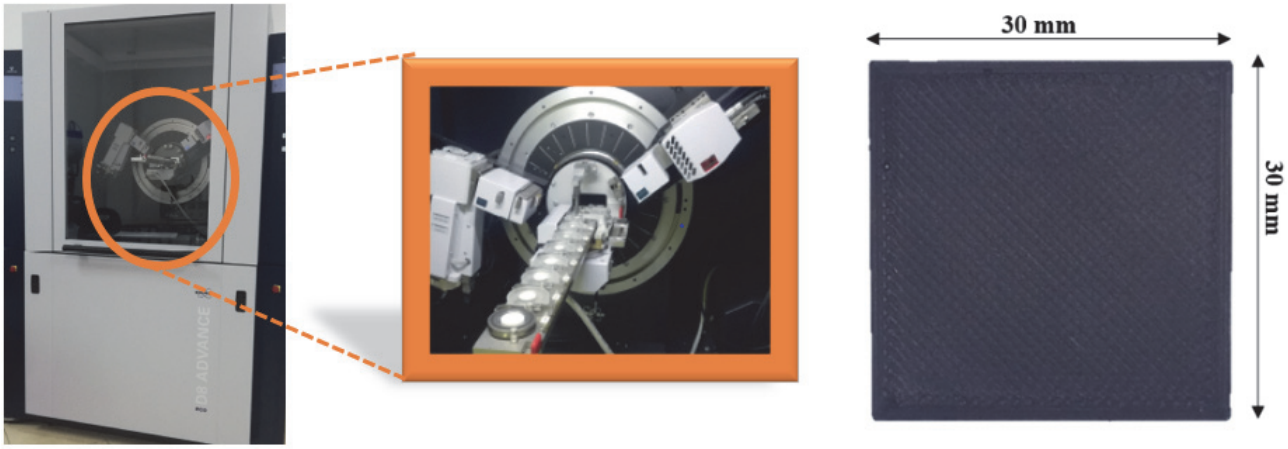

a) b)

Figure 1: a) BRUKER-AXS D8 diffractometer, b) Sample of PLA-CB printed in square form for X-ray testing.

Tensile tests & 3D Printing Process

The process of preparing specimens for tensile testing using 3D printing involves a number of key steps that guarantee the quality and reliability of the results. Firstly, the choice of PLA conductive material is essential: it must be of good quality and adapted to 3D fused deposition modeling (FDM). Secondly, the choice of specimen dimensions for tensile tests is crucial to obtaining reliable and representative results of the mechanical properties of the material. It is essential that the dimensions are adapted to both the specific characteristics of the material tested and the requirements of the machine used. In this paper, every sample is oriented and printed in accordance with ASTM D638 Type 1in Fig. 2 to ensure comparable characteristics between tests. And finally, the choice of the printing parameters is carefully defined: the melting temperature is set at 230 °C, the printing speed is set at 40 mm/min, the platform temperature was around 60 °C, the layer thickness is set at 0.2 mm and the density is set at 100% to guarantee the homogeneity of printed samples.

The 3D sample was created in CATIA, then exported in STL format. It was then loaded into FlashPrint to define the print parameters for the FDM machine and carry out the slicing process [18], [19]. The FDM command was then exported for printing samples. The direction of printing was set at 45° with maximum density to maximize mechanical performance and limit variations due to internal defects or porosity. After each print, the samples were cooled under ambient conditions to stabilize their properties prior to tensile testing. The conductive PLA samples were 3D printed using the FLASHFORGE 3 PRO 3D printer, as shown in Fig. 3.

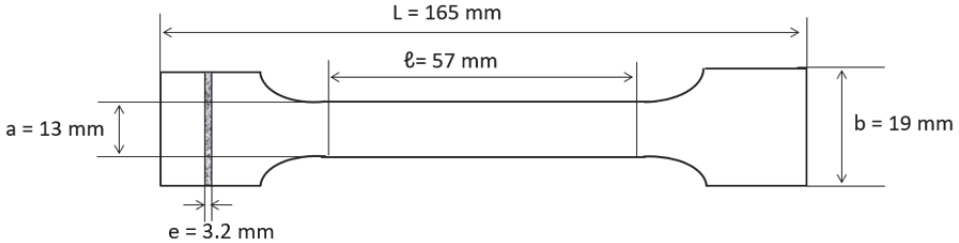

Figure 2: Dimensions of specimens printed according to the ASTM D638 Type 1 standard.

For the experimental part, the samples were 3D printed in order to test their mechanical behavior and analyze their reliability under different tensile speeds using an MTS tensile testing machine with a maximum loading of 30 kN. For this purpose,

we printed 5 samples of uniform dimensions and geometry in PLA-CB for each speed. Crosshead speeds were set at 5, 10, 15, 20, 25, 50, 70, 100, 150 and 200 mm/min, corresponding to respective strain rates of 0.0877, 0.1754, 0.2631, 0.3508, 0.4385, 0.8771, 1.228, 1.7543 and 3.5087 s^{-1}. A total of 50 samples were tested to ensure good repeatability and minimize experimental errors. Fig. 4 presents two images: Fig. 4a showing multiple fractured samples after the tensile test and the Fig. 4b capturing a sample undergoing testing in the tensile machine.

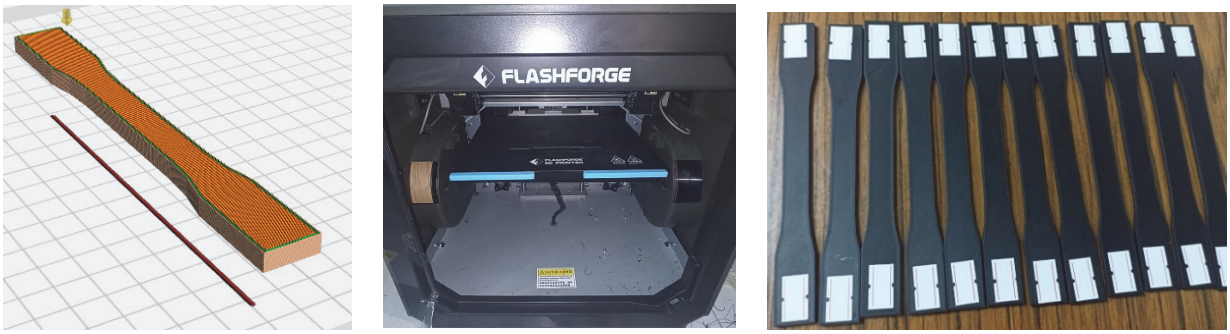

a) b) c)

Figure 3: a) Arrangement of model specimen under Flashprint software; b) 3D printing machine; c) A series of 3D-printed specimens.

a) b)

Figure 4: a) A set of fractured printed samples; b) A sample under tensile test loading.

In a second study, we used Single Edge Notched Tension (SENT) specimens to assess the mechanical behavior of 3D-printed PLA-CB under different notch configurations, including U-, V- and hole-shaped notches. These different notch geometries were selected to examine their impact on mechanical strength and crack propagation in SENT specimens. The specimens were fabricated using the fused filament deposition (FDM) technique too, while maintaining constant printing parameters to ensure comparability of results. This study determined how each type of notch influences crack stability, fracture toughness, and the overall mechanical behavior of the studied material, contributing to a better understanding of the anisotropic properties of 3D-printed PLA-CB. For this study, a series of specimens was printed with different notch configurations: single U, single V, double U, double V, as well as specimens with a central hole as shown in Fig. 5. To ensure repeatability and reliability of results, five specimens were produced for each notch configuration, for a total of 25 specimens. Fig. 6a shows the printed specimens before the tensile tests, while Fig. 6b illustrates the same specimens after the tensile tests and Fig. 6c displays a specimen undergoing testing on the tensile test machine.

Morphology analysis by Scanning Electron Microscopy (SEM) and Energy Dispersive Spectrometer (EDS)

The surface morphologies of PLA-CB were observed using a scanning electron microscope with microanalyzer (SEM-EDS) from HIROX model SH-5500P. SEM analysis was carried out on the fracture surfaces of specimens exposed to tensile tests, in order to assess their failure mechanisms and characterize their ruptured surfaces microscopically. For this purpose, a

representative set of specimens was selected for 3D printing orientation 0 and 45. Prior to SEM analysis, the specimens were cut to an appropriate size for the SEM chamber (1cm x 1cm), then cleaned with alcohol to remove any dust. After that, the specimens were sprayed with Au-Pd using Denton Vacuum Desk V (Denton Vacuum, U.S.A.) machine to create a conductive surface to avoid charge build-up under the electron beam. The pellets were then photographed at different magnifications with an EDS area scan captured by the SEM, targeting the C and O elements.

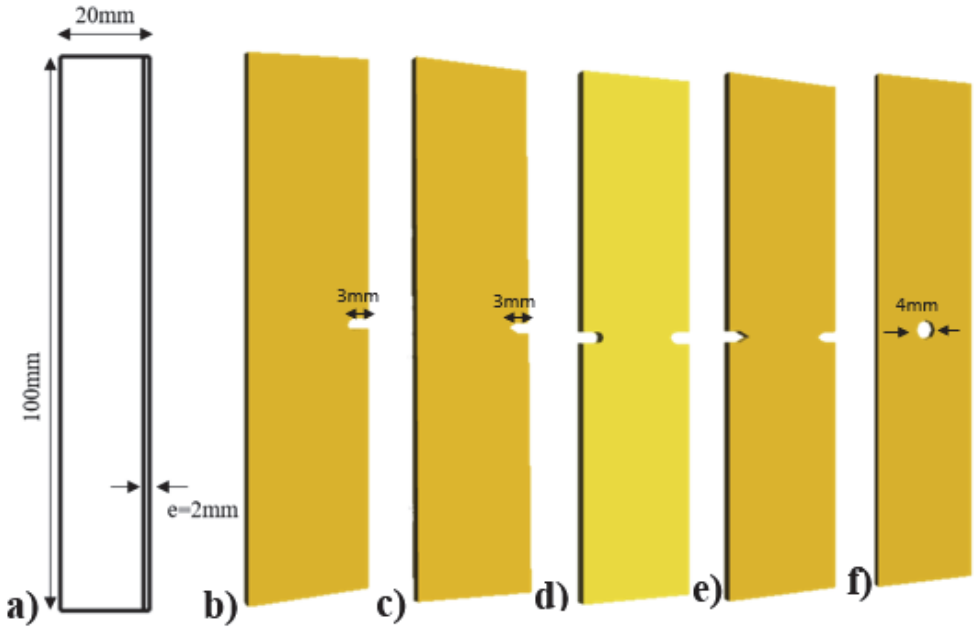

Figure 5: Geometries and dimensions of all notched specimen. a) SENT Specimen dimensions. b) Specimen with a single U-notch. c) Specimen with a single V-notch. d) Specimen with a double U-notch. e) Specimen with a double V-notch. f) Specimen with a central hole.

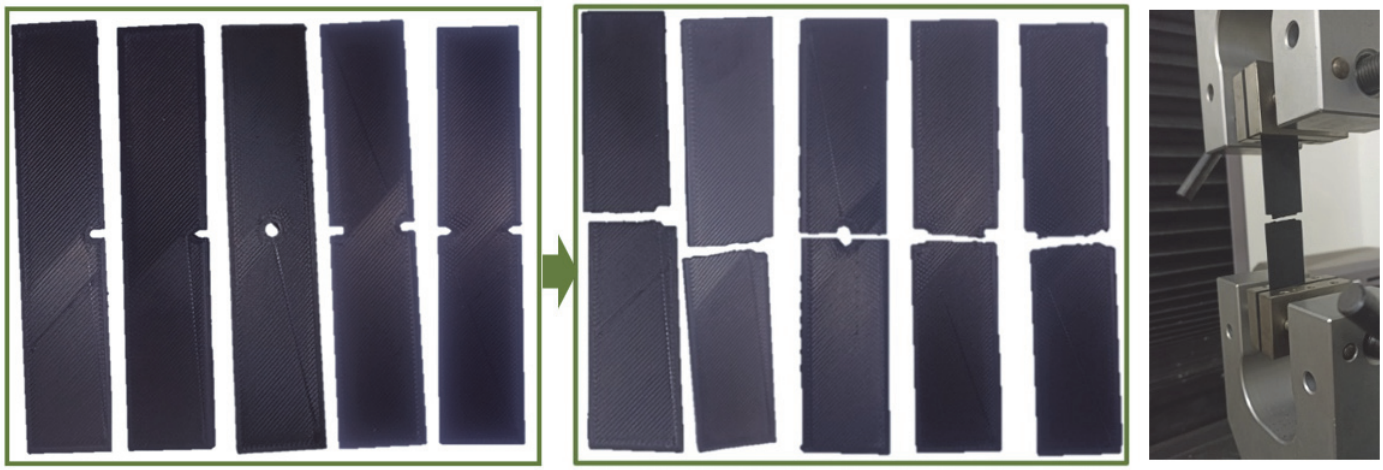

a) b) c)

Figure 6: a) Printed specimens for tensile test. b) Specimens after rupture. c) One Specimen under tensile testing via MTS Testing Machine.

THEORY

According to theory, the Weibull distribution is a probabilistic approach generally used to estimate the relative importance of different variabilities influencing reliability in studies based on fracture resistance [20], [21]. In this study, the two-parameter Weibull distribution was used, i.e. the form factor (m) and scale factor (η), to analyze the

reliability of PLA-CB for both samples tested at different crosshead speeds and samples with different types of notches. The basic form of the cumulative probability density F (x; m, η) that can be obtained from experiments is as follows:

$$F(x; m, \eta) = 1 - \exp(-(x/\eta)^m)) \quad (1)$$

In this work, x-values represent the stress or strain at fracture, allowing us to estimate the reliability of structural and mechanical components. In addition, material behavior is influenced by two main factors, damage (D) and reliability (R). Damage represents the physical degradation or fatigue that a material can accumulate, while reliability reflects its ability to operate efficiently over a defined period. The interaction of these two factors gives the expected service life of the material. Probability of failure and probability of survival relationship can be expressed mathematically to demonstrate the overall durability of the material as below:

$$F(x; m, \eta) + R(x; m, \eta) = 1 \quad (2)$$

So, the probability of survival, is given by:

$$R(x; m,\eta) = exp(-(x/\eta))^m \quad with \quad m \geq 0 \text{ and } \eta \geq 0 \quad (3)$$

Weibull distribution parameters can be estimated using several methods, each adapted to specific contexts. The most commonly used approaches are linear regression, method of maximum likelihood and the least squares method. In the context of this work, the linear regression method was chosen to estimate the Weibull parameters. This choice is based on its ease of application and its ability to provide reliable results with the available data.
The linear regression model is written as Y = mX + c and is obtained by rearranging Eqn. (1) and adding the logarithms twice on both sides, as follows:

$$Ln(\ln(1/(1- F(x; m,\eta)))) = m \ln(x) - m \ln(\eta) \quad (4)$$

F (x; m, η) is estimated from experimental stress and strain values by ranking the ' N ' observations in ascending order of magnitude.
The estimates for m and nu are obtained by linear regression of (X, Y), such as X=ln(x) and

$$Y = \ln(\ln(1/(1- F(x; m, \eta))))$$

from the model in Eqn. (4). The slope of the line providing the shape parameter ' m ' and the scale factor value ' η ' is determined from the point of intersection of the regression line and the Y-axis. The shape parameter (also called Weibull modulus), describes how the data from the distribution are spread. This parameter directly influences the shape of the probability curve. The scale parameter corresponds to the range of the data in the distribution. It is directly linked to the maximum amplitude, enabling us to situate the data on the stress or strain scale, and gives an idea of the average capacity of the material before it fails.

RESULTS AND DISCUSSION

Crystal structure Analysis

X-rays disperse in different directions when they intersect the crystal plane, making it possible to analyze angles, crystal orientation, the proportion of crystalline phases and the intensity of diffracted rays using XRD technology [22], [23]. In Fig. 7, we show the diffraction pattern of PLA reinforced with conductive Carbon Black fillers on a specimen with a square dimension of 30 mm and a thickness of 0.2 mm. The broad slope observed in the lower corner region (below 2θ = 20◦) represents the amorphous phase in the composite. That explains the presence of Carbon black, which is mainly characterized by an amorphous nature. This is associated to the absence of a clear crystalline peak typically linked to the crystallographic plane. As a general rule, the crystallization process of pure PLA is too slow to produce noticeable crystallinity, particularly under non-isothermal conditions. In the sample studied, a clear crystalline peak was observed at 20,5701◦ corresponding to the (100) crystal plane. PLA-CB then showed two peaks at 2θ = 28.365◦ which is attributed to the (110) and (200) crystal planes and 2θ = 42.4541◦ that allocated to the crystal plan (101).

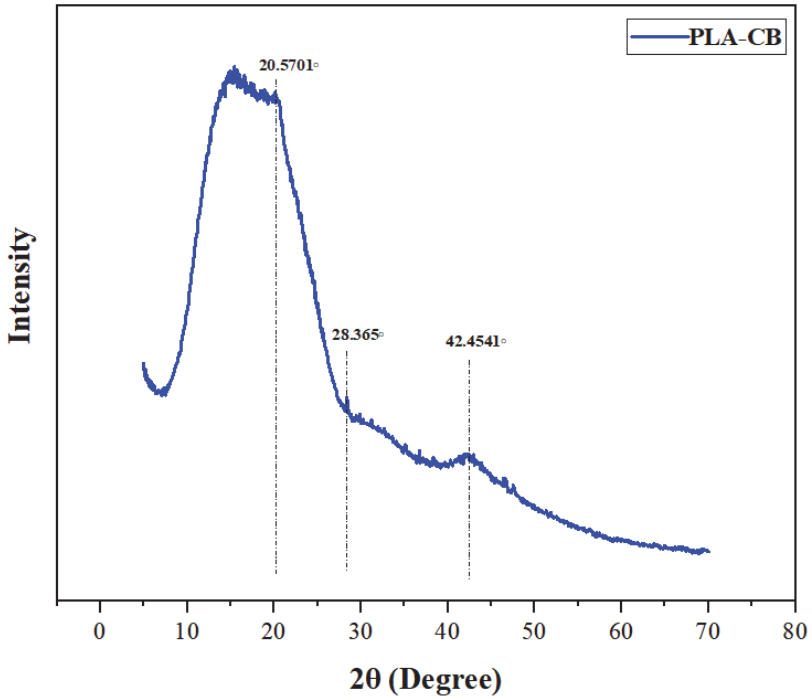

Figure 7: XRD curve of PLA-CB composite.

Morphological characteristics analysis of PLA/CB

Scanning electron microscopy was performed on the fracture surfaces of 3D-printed specimens submitted to tensile tests with different layer Orientations (0 ° and 45 °). The Fig. 8 shows SEM images of PLA-CB with 0° Orientation (Fig. 8a) at x88 magnification and with 45° Orientation (Fig. 8b) at x88 and x200 magnification. The sample was then processed by EDS to create a mapping for visualizing the distribution of carbon black in PLA. Fig. 8c shows the EDS mapping with a color profile for two printed PLA-CB samples tested, demonstrating the presence of carbon black over the whole surface. CB is therefore distributed regularly in the PLA matrix, making it ideal for the construction of a conductive structure.

The broken samples were examined to reveal their microstructural characteristics. The results of PLA-CB tensile tests depend on the compatibility of the CB fibers in the PLA matrix. The analysis of the microstructure provides information on adhesion at the interface between the fibers and the matrix, as well as on the distribution of the fibers within the PLA matrix. The SEM image of the PLA-CB sample with 0 orientation (where the layers are in parallel with the tensile direction), shown in Fig. 8a, demonstrates relatively smooth surfaces with zones of brittle fracture, characterized by glossy facets and a marked absence of plastic deformation and few visible bonds between layers. However, a few pores can be observed, indicating the brittle characteristics of the material, which has been reported by some previous studies[24], [25]. In contrast, the Figs. 8b of PLA-CB samples with orientation 45 reveals a stronger fracture, with more irregular surfaces and more visible pores, attesting to reinforced adhesion between the layers and clear signs of better interactions or stronger bonds between the layers. In this configuration, failure does not follow a single direction, but is influenced by the inclined orientation of the layers, resulting in a mixed failure mode. Signs of plastic deformation are often more pronounced, reflecting greater energy absorption prior to fracture. Comparatively, specimens printed at 45° exhibit superior mechanical behavior under tension, showing much more significant deformation before rupture and more complex surfaces.

Crosshead Speed and notch effects on uniaxial tensile properties - Influence of crosshead speed on tensile properties of PLA-CB

The influence of crosshead speed and strain rate on PLA-CB is represented by the stress-strain curve in Fig. 10. For each speed, we have included error bars demonstrating the standard deviation calculated from the five tested samples in order to better illustrate the variety in the results. These error bars increase the dependability of our study and offer a more transparent representation of data dispersion. As crosshead speed increases, breaking stress rises progressively from 19.30134 MPa for a low speed of S=5mm/min to 27.27714 MPa for a speed of S=200mm/min according to the Tab. 2, reflecting an increase in rigidity. So, the material may support more stress while becoming less flexible and reaching its breaking point faster. However, this increase in stress is accompanied by a reduction in the breaking elongation, from 8% to 5.7046% as shown in Fig. 9. This tendency is explained by the fact that at higher speeds, the time for reorganization and

alignment of polymer chains under stress becomes limited, which increases the material's strength and reinforces its fracture toughness. In contrast, at lower speeds, the material has more time to restructure its polymer chains, leading to increased ductility and have a progressive transition to fracture. This is due to the presence of Carbon Black, which increases PLA's rigidity and reduces its capacity for deformation thanks to its conductive fillers that limit the mobility of polymer chains. As a result, the PLA-CB fails at a higher stress level with less deformation under rapid loading conditions.

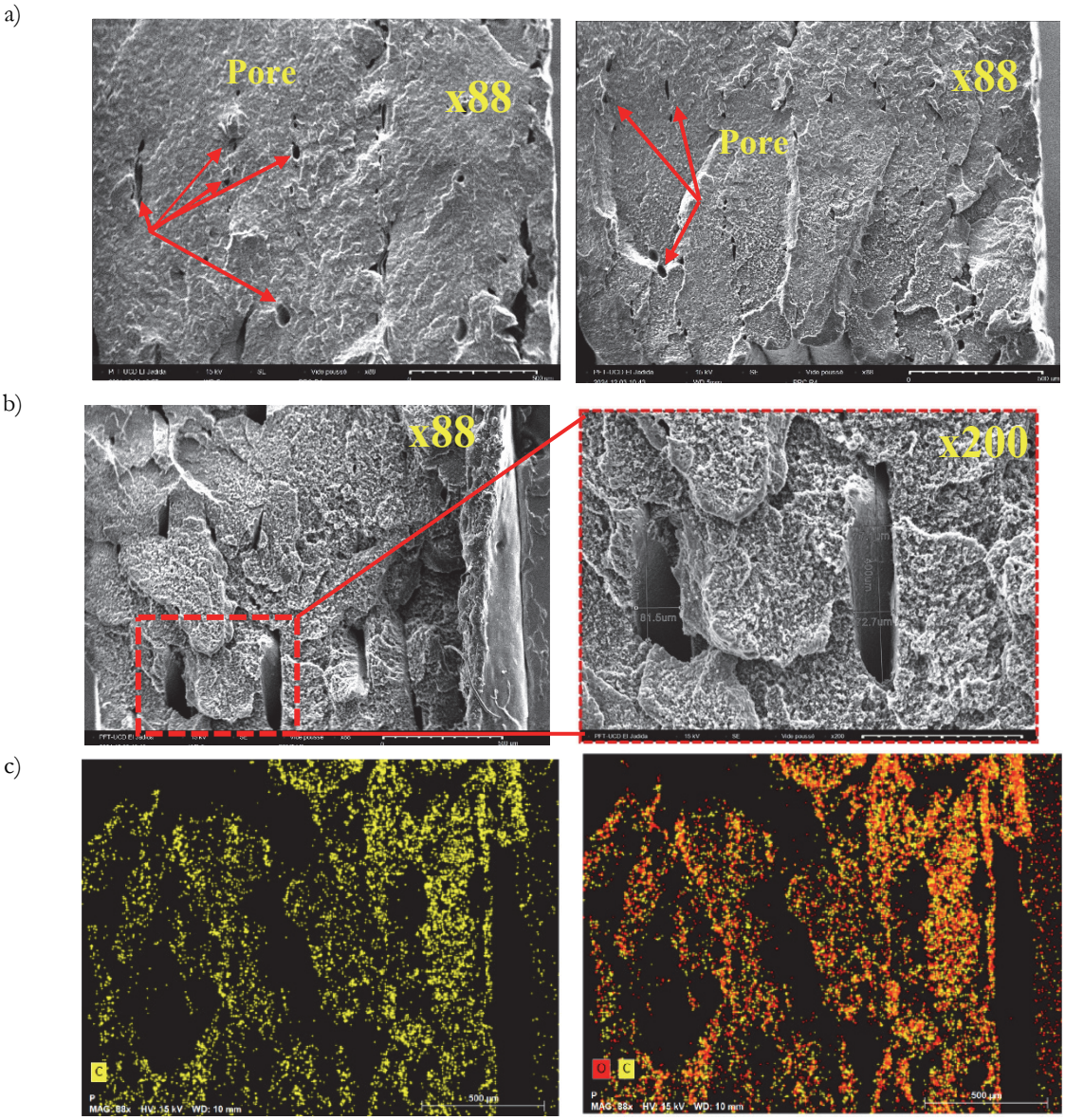

Figure 8: SEM images of the fracture surface after tensile testing (scale bar is 500 µm). a) With 0° orientation at 88x magnification. b) With 45° orientation at 88x and 200x magnification. c) Mapping the distribution of C and O elements in a sample.

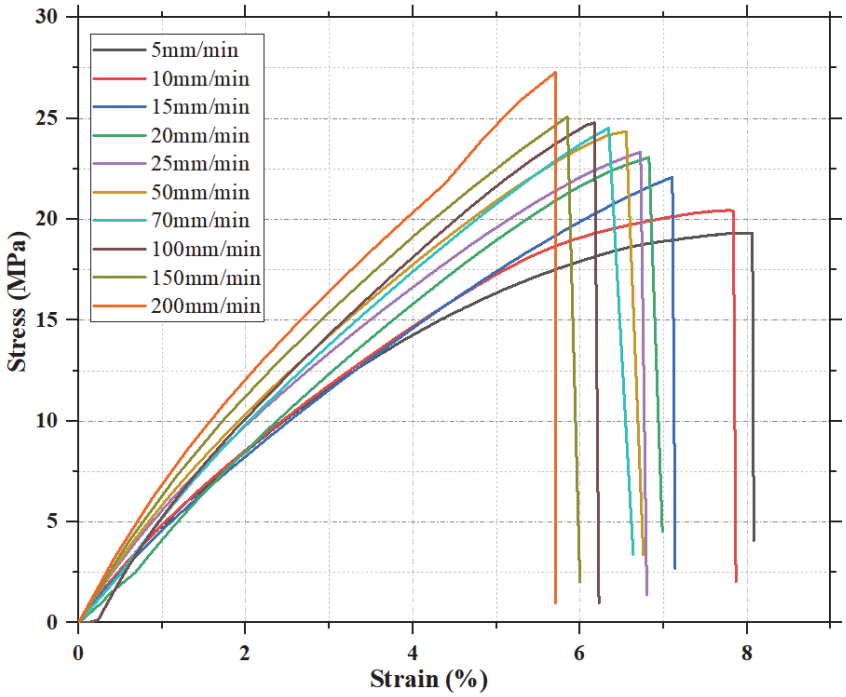

Figure 9: The effect of crosshead speed on the stress-strain curves of conductive PLA printed samples.

Crosshead Speeds (mm/min)	5	10	15	20	25	50	70	100	150	200
Maximal stress (MPa)	19.315	20.436	22.067	23.061	23.319	24.347	24.522	24.781	25.075	27.277
Breaking strength (MPa)	19.301	20.416	22.067	23.061	23.319	24.347	24.522	24.781	25.075	27.277
Elongation (%)	8.065	7.836	7.105	6.826	6.726	6.554	6.344	6.176	5.851	5.704

Table 2: Effects of crosshead speed on the mechanical characteristics of conductive PLA.

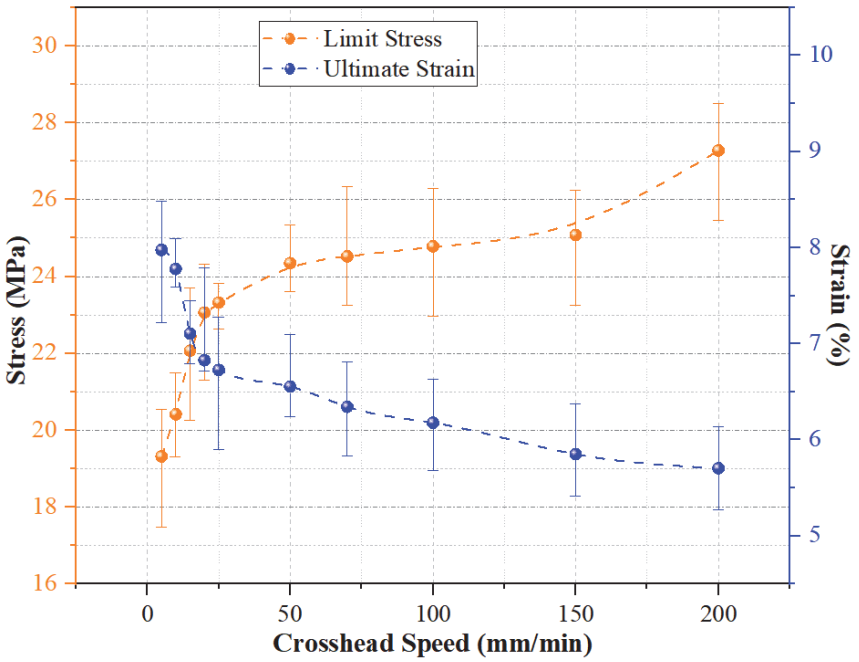

Figure 10: Progression of stress-strain based on crosshead speeds evolution on PLA-CB.

Influence of different notches on tensile characteristics of PLA-CB

Fig. 11 shows the tensile curves obtained for 3D-printed SENT specimens of PLA-CB with different notch geometries (single U, single V, double U, double V and a central hole) to study the influence of stress concentration on the mechanical behavior of the material. The curves of simple U- and V-notched specimens show that simple U- and V- notches, producing unidirectional weak points, present slightly distinctive behaviors: the U-shaped notches, thanks to their rounded configuration, distribute stresses more efficiently, leading to increased stress rupture and significant deformation prior to failure. On the other hand, V-shaped notches, thanks to their sharp angles, concentrate stresses more intensively, reducing strength and leading to slightly more brittle fracture than the U-shaped notch. This impact is amplified by double notches (U or V), which create two zones of stress concentration, making the material more susceptible to early failure, especially in the case of V-notches. Finally, the samples with the center hole, showing a radial distribution of stresses around the hole, indicates a limitation of fracture that is directly related to the size of the hole, which is 4mm in diameter compared to its width of 20mm. This configuration resulted in progressive fracture, which is generally more significant than single and double U- and V-notches form. In addition, comparing notched specimens to virgin one under tensile testing reveals a clear shift in the material's behavior from ductile to brittle. The notched specimens fractured much faster than the unnotched one and showed almost no significant deformation, with the plastic zone almost disappeared. Consequently, geometries in 3D printed elements have a very important impact on the mechanical strength of the material. The values for maximum - strain just before break related to each notch geometry are shown in Tab. 3.

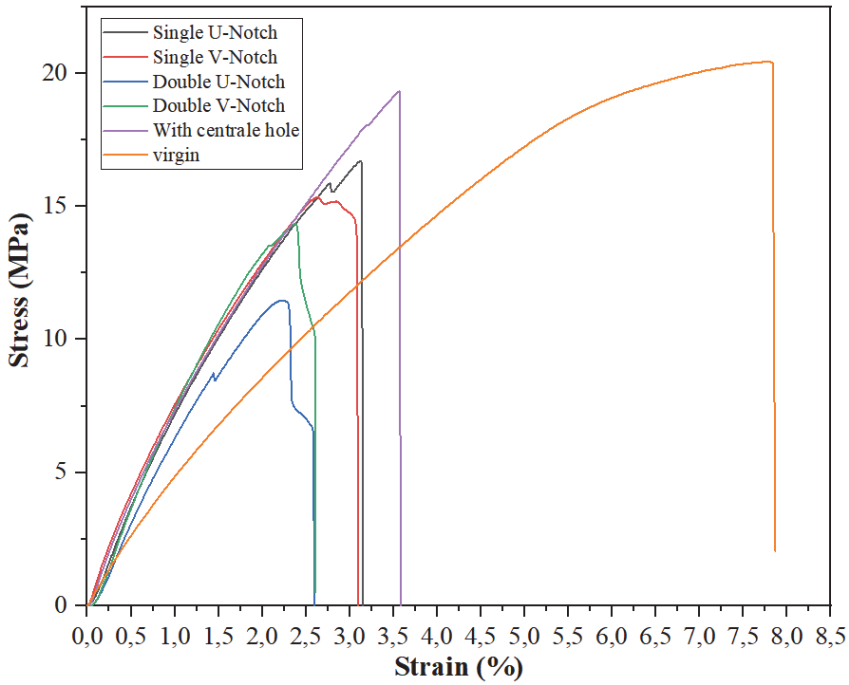

Figure 11: The effect of Different Notches on the stress-strain curves of conductive PLA printed samples.

Type of Notch	Single U-Notch	Single V-Notch	Double U-Notch	Double V-Notch	Specimen with center hole
Maximal stress (MPa)	16.6985	15.356	11.4682	14.3515	19.3358
Breaking strength (MPa)	16.6209	13.748	6.546	9.9814	19.3358
Elongation at Break (%)	3.1392	3.0833	2.5835	2.6059	3.5693

Table 3: Effects of notches on the mechanical characteristics of PLA-CB.

Weibull Distribution

Figs. 12 and 13 show the tendencies in tensile strength and breaking strain for different specimens tested under the effects of crosshead speed and under the effects of notches. The shape and scale parameters of Weibull's distribution function have

been calculated for tensile strength and breaking strain from the linear regression equations, and their values are shown in Tabs. 4 and 5.

For the linear regression curves of crosshead speed on tensile stress, the shape factor of 11.774 indicates low stress dispersion at break, while the high scale factor at 24.427 represents good mechanical strength, indicating that the increase in crosshead speed is beneficial for the strength of PLA-CB. On the other hand, the effect of notches with a shape factor of 6.0903 shows a significant variability in stress, which is normal due to the concentration of stress through the local effects of the notches. In addition, the scale factor is 16,589 lower than the one observed for the speed effect 24.427. This is due to a reduction in overall strength as notching weakens the material and reduces its durability.

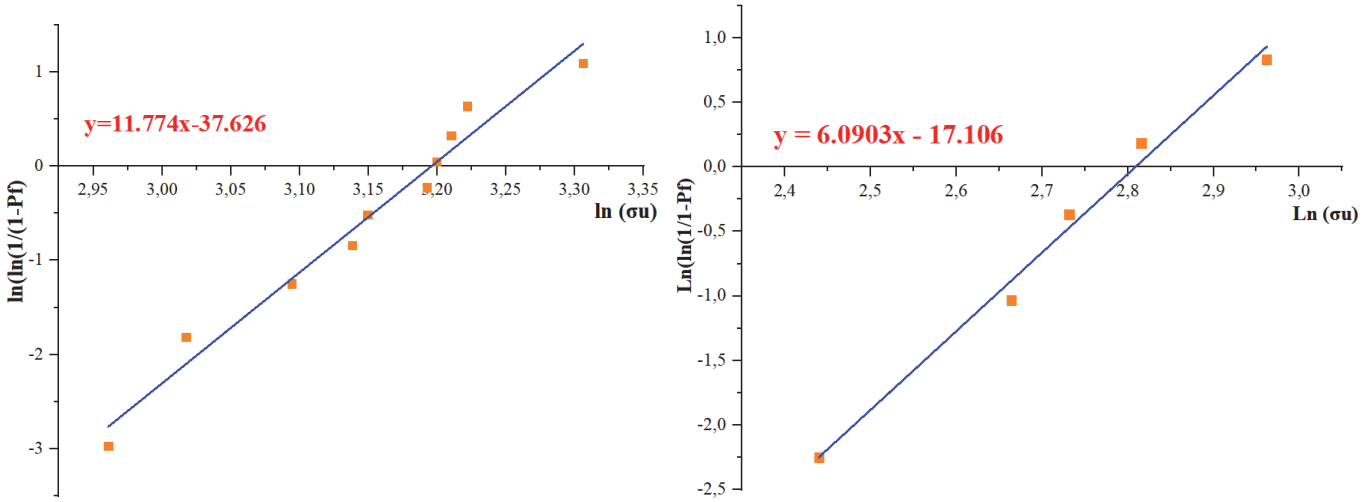

Figure 12: Weibull fitting of experimental PLA-CB tensile Stress data. a) Crosshead speed effect b) Notches effect.

Weibull Parameters	Crosshead speed effect	Notches effect
Related Equation	Y=11.774x –37.626	Y=6.0903x – 17.106
Shape parameter (m)	11.774	6.0903
Scale parameter (η)	24.427	16.589

Table 4: Experimental values of Weibull parameters for tensile strength.

Regarding strain, it can be seen that speed effect has a beneficial impact on the material, presenting a shape factor of 10.509 which indicates limited strain distribution in case of break and structural regularity. The capacity of significant strain before breaking is indicated by the reduced scale of 7.025. However, the impact of notches is clearly unfavorable, showing a low shape coefficient of 5.7368, reporting high diversity in deformation at break, and an extremely low scale of 3.003, indicating considerably reduced ductility. As a result, PLA-CB is better adapted to fast dynamic loads, although prudent printing is needed to reduce any sources of stress concentration such as notching.

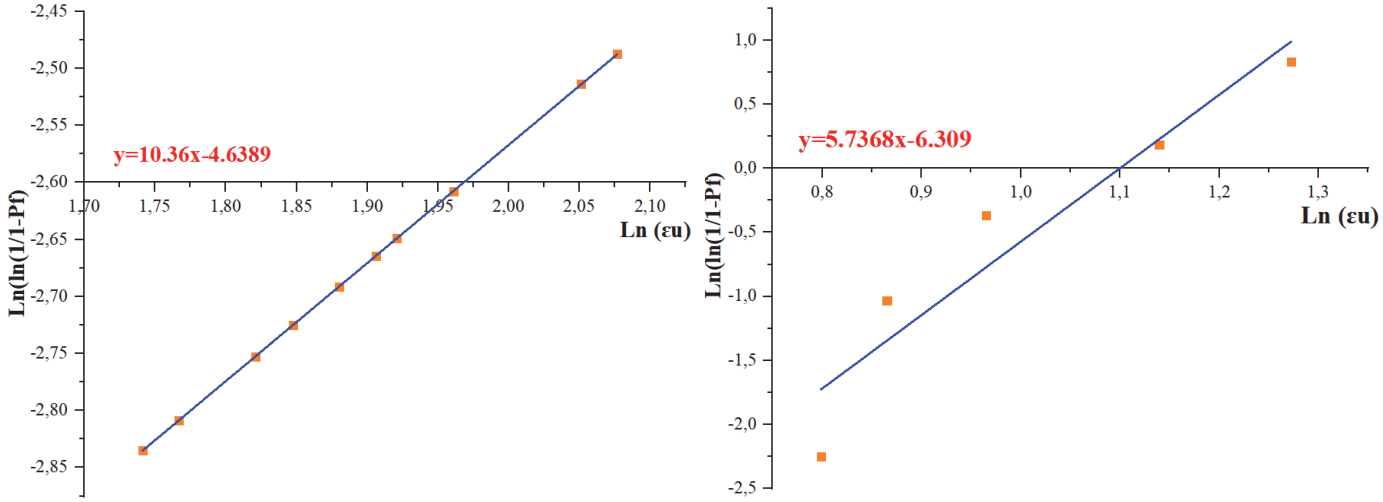

Figure 13: Weibull fitting of experimental PLA-CB tensile Strain data. a) Crosshead speed effect b) Notches effect.

Weibull Parameters	Crosshead speed effect	Notches effect
Related Equation	Y=10.509x – 20.488	Y=5.7368x – 6.309
Shape parameter (m)	10.509	5.7368
Scale parameter (η)	7.025	3.003

Table 5: Experimental values of Weibull parameters of strain at failure.

Figs. 14 and 15 illustrate the PLA-CB density probability function for stress and strain responding to crosshead speed and notches. Regarding stress, the crosshead speed curve shows a narrow range, oriented towards a high stress of 22.067, indicating satisfactory homogeneity and increased strength with increasing load. This suggests that the studied material reacts reliably and it is able to resist significant stresses under dynamic conditions. On the other hand, the notch curve is more extensive and oriented towards lower stresses than that shown for speed, indicating significant dispersion and a reduction in strength of 14.351. Therefore, notches represent zones of critical brittleness, making failure less predictable.

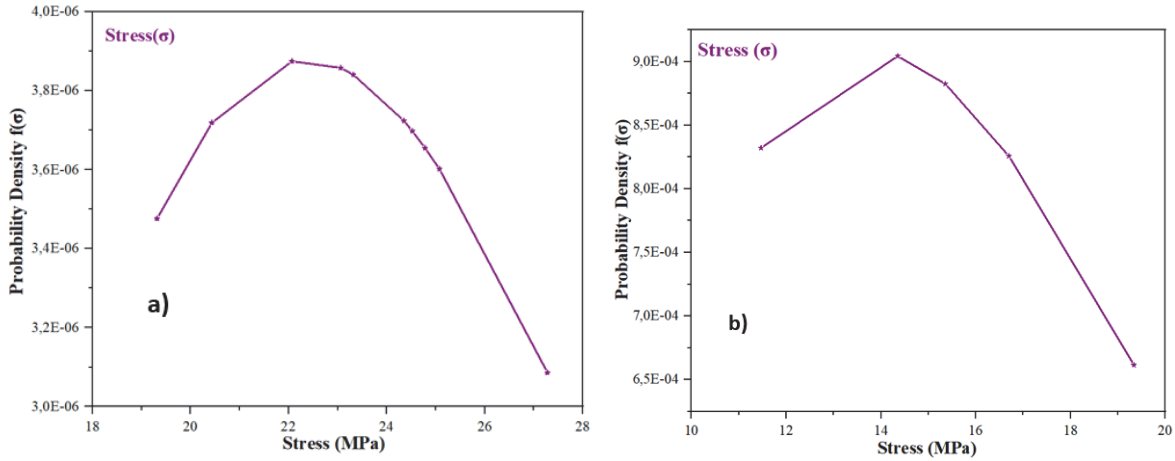

Figure 14: Evolution of stress probability density. a) Crosshead speed effect b) Notches effect.

A similar pattern is observed for strain in Fig. 15: the crosshead speed effect curve shows a narrow, moderately centered curve, indicating that the material has a certain capacity to deform before breaking of around 6.344%, with relative homogeneity. In contrast, notches generate a very wide curve, displaced towards low deformations, indicating much reduced ductility and early rupture of 2.375%.

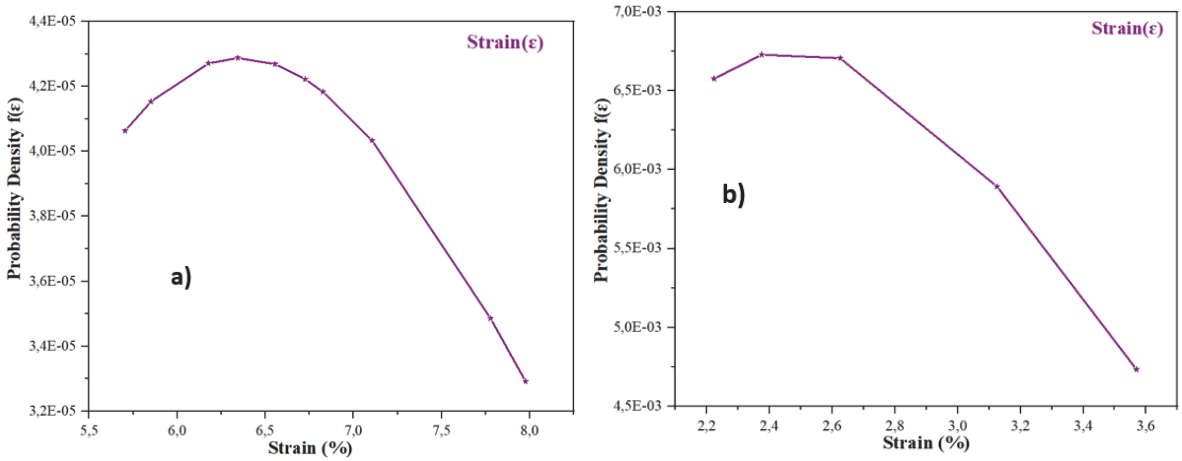

Figure 15: Evolution of strain probability density. a) Crosshead speed effect b) Notches effect.

The knowledge of the probability of survival and failure leads to an assessment of the risk of material damage. Figs. 16 and 17 represent the survival and failure probability curves for analyzing the effect of crosshead speed and the effect of notches

on printed PLA-CB as a function of stress and strain. Each graph represents two curves, the first in green representing the probability of the material functioning properly, and the second in blue representing the probability of failure. The intersection between the two curves marks the critical stress or strain where the probability of survival and failure are equal to 50%. Before this limit (σ_c; ε_c), the material in Zone I of stable performance, resisting stresses well, meaning that the material can support these stress levels without significant risk of failure. After this point, the material enters into Zone II of vulnerability, where the risk of failure dominates, either under excessive stresses or strains. This is the breaking zone, where deformation exceeds tolerable levels and reaches the material's plastic or brittle limit, eventually leading to failure.
The Ps-P_f graphs show that speed increases PLA-CB strength and stiffness, pushing the critical intersection limit to higher values. In contrast, notches considerably reduce the survival zone and increase the probability of failure at low stresses and strains.

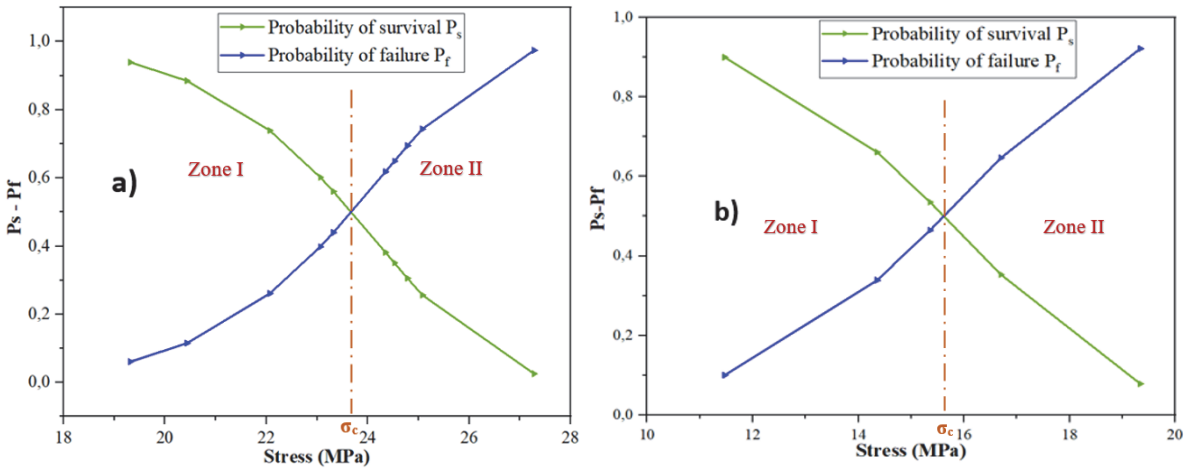

Figure 16: Probability of survival Ps and probability of failure Pf as a function of stress. Crosshead speed effect b) Notches effect.

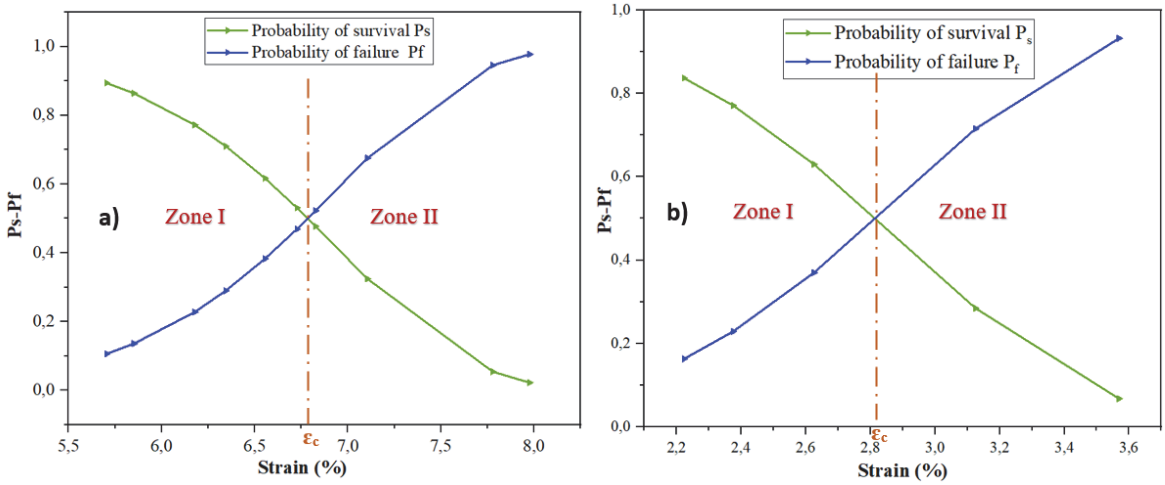

Figure 17: Probability of survival P_s and probability of failure P_f as a function of stress. Crosshead speed effect b) Notches effect.

CONCLUSION

This experimental study focuses on a deterministic and probabilistic approach to estimate the experimental damage of the PLA-CB composite material. Key characteristics, such as strength and strain at break, are determined by the number of defects present in the material, considering the effects of tensile speed, notch geometry, and layer orientation in 3D-printed PLA-CB. The Weibull analysis presented in this study is used to determine probabilistic values for ultimate strength and strain, which represent the critical load level requiring intervention. This is when the material reaches Stage II of accelerated damage, where deformation exceeds the material's tolerable limits, reaching the plastic and brittle thresholds, ultimately leading to fracture. The results show that tensile speed, notch geometry, and layer orientation

significantly affect the material's mechanical performance. Specifically, higher tensile speeds increase fracture toughness but reduce ductility, while variations in notch geometry and orientation influence stress concentration and fracture mechanisms.

NOMENCLATURE

PLA : Polylactic Acid
CB : Carbon Black
FDM : Fused Deposition Modelling
FFF: Fused Filament Fabrication
ICPs : Intrinsically Conductive Polymers
PCCs : Conductive Polymer Composites
SEM : Scanning Electron Microscopy
EDS: Energy Dispersive Spectrometer
XRD : X-Ray diffraction
m : Weibull shape factor
η : Weibull scale factor
F : Damage and Weibull Failure
R: Reliability and Weibull Reliability
P_s : Probability of survival
P_f : Probability of failure
σ_c : Critical Stress
ε_c : Critical Strain

REFERENCES

[1] Chu, H., Chen, Z., Chen, Y., Wei, D., Liu, Y. and Zhao, H. (2024). Mechanical Properties and Crystallinity of Specific PLA/Cellulose Composites by Surface Modification of Nanofibrillated Cellulose. Polymers, 16(17). DOI: 10.3390/polym16172474.

[2] Senokos, E., Ou, Y., Torres, J. J., Sket, F., González, C., Marcilla, R. and Vilatela, J. J. (2018). Energy storage in structural composites by introducing CNT fiber / polymer electrolyte interleaves, pp. 1–10. DOI: 10.1038/s41598-018-21829-5.

[3] Yan, T., Ye, X. C., He, E., Gao, Q., Wang, Y., Gong, L., Ye, Y. and Wu, H. (2024). Preparation of a double-layer bionic bamboo structure absorber based on CB/PLA-TPU composites and its broadband microwave absorption characteristics. Journal of Alloys and Compounds, 990. DOI: 10.1016/j.jallcom.2024.174461.

[4] Kwok, S. W., Goh, K. H. H., Tan, Z. D., Tan, S. T. M., Tjiu, W. W., Soh, J. Y., Ng, Z. J. G., Chan, Y. Z., Hui, H. K. and Goh, K. E. J. (2017). Electrically conductive filament for 3D-printed circuits and sensors. Applied Materials Today, 9, pp. 167–175. DOI: 10.1016/j.apmt.2017.07.001.

[5] Kumar Mishra, P. and P, S. (2020). Prediction of in-plane stiffness of multi-material 3D printed laminate parts fabricated by FDM process using CLT and its mechanical behaviour under tensile load. Materials Today Communications, 23, 100955. DOI: 10.1016/j.mtcomm.2020.100955.

[6] Wang, Z., Hensleigh, R., Xu, Z., Wang, J., Park, J. J. and Papathanasopoulos, A. (2025). Ultra-light antennas via charge programmed deposition additive manufacturing. Nature Communications. DOI: 10.1038/s41467-024-53513-w.

[7] Khalifa, M., Lammer, H., Gadad, M. S., Varsavas, S. D. and Weng, Z. (2025). Recent advances on copper/polymer nanocomposites: Processing strategies, mechanisms, and antibacterial efficacy. European Polymer Journal, 223, 113637. DOI: 10.1016/j.eurpolymj.2024.113637.

[8] Panwar, V., Sachdev, V. K. and Mehra, R. M. (2007). Insulator conductor transition in low-density polyethylene-graphite composites. European Polymer Journal, 43(2), pp. 573–585. DOI: 10.1016/j.eurpolymj.2006.11.017.

[9] Arora, N., Dua, S., Singh, V. K., Singh, S. K. and Senthilkumar, T. (2024). A comprehensive review on fillers and mechanical properties of 3D printed polymer composites. Materials Today Communications, 40, 109617. DOI: 10.1016/j.mtcomm.2024.109617.

[10] Liesenfeld, J., Jablonski, J. J., da Silva, J. R. F., Buenos, A. A. and Scheuer, C. J. (2024). Impact of annealing on the characteristics of 3D-printed graphene-reinforced PLA composite. Journal of Manufacturing Processes, 128, pp. 133–157. DOI: 10.1016/j.jmapro.2024.08.025.

[11] Chen, X., Yan, W., Mathivanan, M., Chen, H., Lambourne, A., Gill, V. and Hu, X. (2022). Thermally conductive polymer composites for thermal management of electric machines: A modeling and experimental study. Materials Today Communications, 32, 104018. DOI: 10.1016/j.mtcomm.2022.104018.

[12] Wei, Q. Y., Fang, Y. D., Sun, Z. B., Zeng, Y., Zhang, J., Lei, J., Xu, L., Lin, H., Zhong, G. J. and Li, Z. M. (2023). Fabrication of PLA/CB composites with excellent electrical conductivity and stiffness-ductility balance based on coupling extensional stress with thermal field. Composites Part A: Applied Science and Manufacturing, 169. DOI: 10.1016/j.compositesa.2023.107516.

[13] Choudhury, S. N., Das, P., Bhawal, P., Pal, A., Banerji, P. and Das, N. C. (2023). Double percolation behavior through the preferential distribution of conductive black in polymer blends to boost electrical properties and EMI shielding effectiveness. Materials Today Communications, 35, 106109. DOI: 10.1016/j.mtcomm.2023.106109.

[14] Alarifi, I. M. (2019). Investigation the conductivity of carbon fiber composites focusing on measurement techniques under dynamic and static loads. Journal of Materials Research and Technology, 8(5), pp. 4863–4893. DOI: 10.1016/j.jmrt.2019.08.019.

[15] Hachimi, T., Naboulsi, N., Majid, F., Rhanim, R., Mrani, I. and Rhanim, H. (2021). Design and Manufacturing of a 3D printer filaments extruder. Procedia Structural Integrity, 33(C), pp. 907–916. DOI: 10.1016/j.prostr.2021.10.101.

[16] Naboulsi, N., Hachimi, T., Majid, F., Rhanim, R., Zekriti, N. and Rhanim, H. (2021). Modeling and control of 3D filament extruder. Procedia Structural Integrity, 33(C), pp. 989–995. DOI: 10.1016/j.prostr.2021.10.109.

[17] Horst, D. J., de Andrade Junior, P. P., Duvoisin, C. A. and Vieira, R. de A. (2020). Fabrication of conductive filaments for 3d-printing: Polymer nanocomposites. Biointerface Research in Applied Chemistry, 10(6), pp. 6577–6586. DOI: 10.33263/BRIAC106.65776586.

[18] Hachimi, T., Majid, F., Zekriti, N., Rhanim, R. and Rhanim, H. (2024). Improvement of 3D printing polymer simulations considering converting G-code to Abaqus. International Journal of Advanced Manufacturing Technology, 131(9–10), pp. 5193–5208. DOI: 10.1007/S00170-024-13300-9.

[19] Hisham, M., Shebeeb C, M., C, D., Jacob, L. and Butt, H. (2024). Additive manufacturing of carbon nanocomposites for structural applications. Journal of Materials Research and Technology, 28, pp. 4674–4693. DOI: 10.1016/j.jmrt.2024.01.049.

[20] Krumbholz, M., Hieronymus, C. F., Burchardt, S., Troll, V. R., Tanner, D. C. and Friese, N. (2014). Weibull-distributed dyke thickness reflects probabilistic character of host-rock strength. Nature Communications, 5, pp. 1–7. DOI: 10.1038/ncomms4272.

[21] Majid, F. (2020). Probabilistic reliability of thermoplastic piping networks and maintenance strategy choice using Weibull distribution, pp. 1–11. DOI: 10.1002/mdp2.207.

[22] Chu, H., Chen, Z., Chen, Y., Wei, D., Liu, Y. and Zhao, H. (2024). Mechanical Properties and Crystallinity of Specific PLA/Cellulose Composites by Surface Modification of Nanofibrillated Cellulose. Polymers, 16(17). DOI: 10.3390/polym16172474.

[23] Mittal, V., Akhtar, T., Luckachan, G. and Matsko, N. (2015). PLA, TPS and PCL binary and ternary blends: structural characterization and time-dependent morphological changes. Colloid and Polymer Science, 293(2), pp. 573–585. DOI: 10.1007/S00396-014-3458-7.

[24] Khan, A., Sapuan, S. M., Zainudin, E. S. and Zuhri, M. Y. M. (2024). Physical, mechanical and thermal properties of novel bamboo/kenaf fiber-reinforced polylactic acid (PLA) hybrid composites. Composites Communications, 51. DOI: 10.1016/j.coco.2024.102103.

[25] Rasheed, M., Jawaid, M., Parveez, B., Bhat, A. H. and Alamery, S. (2021). Morphology, structural, thermal, and tensile properties of bamboo microcrystalline cellulose/poly(Lactic acid)/poly(butylene succinate) composites. Polymers, 13(3), pp. 1–15. DOI: 10.3390/polym13030465.